Nanoscale

COMMUNICATION

View Article Online
View Journal | View Issue

Cite this: *Nanoscale*, 2016, **8**, 7408

Received 12th December 2015,
Accepted 11th March 2016

DOI: 10.1039/c5nr08832a

www.rsc.org/nanoscale

$Li_3V_2(PO_4)_3$ encapsulated flexible free-standing nanofabric cathodes for fast charging and long life-cycle lithium-ion batteries†

Pingping Sun,‡[a,b] Xueying Zhao,‡[a,c] Renpeng Chen,[a] Tao Chen,[a] Lianbo Ma,[a] Qi Fan,[b] Hongling Lu,[a] Yi Hu,[a] Zuoxiu Tie,[a,d] Zhong Jin,*[a] Qingyu Xu*[b] and Jie Liu*[a,e]

Lithiated transition metal phosphates with large theoretical capacities have emerged as promising cathode materials for rechargeable lithium-ion batteries. However, the poor kinetic properties caused by their low intrinsic electronic and ionic conductivity greatly hinder their practical applications. In this work, we demonstrate a novel strategy to prepare monoclinic lithium vanadium phosphate nanoparticles implanted in carbon nanofibers as the cathodes of Li-ion cells with high capacity, flexibility, long cycle stability and significantly improved high-rate performance. The composite nanofibers were obtained by electrospinning using polyacrylonitrile and $Li_3V_2(PO_4)_3$ nanoparticles, followed by annealing and coating with a thin layer of carbon by plasma enhanced chemical vapor deposition. The $Li_3V_2(PO_4)_3$ nanocrystals with the monoclinic phase were uniformly distributed in the composite nanofibers. The electrochemical performances of the as-prepared binder-free fibrous cathodes were characterized by potentiostatic and galvanostatic tests. At the rate of 0.5 C in the range of 3.0–4.3 V, the composite displayed an initial discharge capacity of 128 mA h g^{-1} (96.2% of the theoretical capacity). A discharge capacity of 120 mA h g^{-1} was observed even at a high rate of 10 C, and a capacity retention of 98.9% was maintained after 500 cycles at 5 C, indicating excellent high-rate capability and capacity retention. Compared to the control samples without a carbon outer-layer, the composite nanofibers with carbon coating demonstrated much better electrochemical performances. It indicates that the carbon coating can further protect the structural integrity of nanofabric electrodes during the charge/discharge processes without hindering the Li-ion mobility and also can prevent undesired side reactions with an electrolyte, thus greatly improving the rate performance and cyclic stability of the cathode.

1. Introduction

Rechargeable lithium-ion batteries (LIBs) are playing an important role in the field of energy storage, owing to their light weight, high energy density and long cycle durability without a memory effect.[1,2] In recent years, LIBs have been rapidly developed for application in portable electronics and electric vehicles.[3–6] Vanadium(v)-based materials, such as $A_2[(VO)_2(HPO_3)_2(C_2O_4)]$(A = K, Na, Li),[7–9] β-$Ag_{0.33}V_2O_5$,[10] and α_I-$LiVOPO_4$,[11], are the widely investigated cathode materials for LIBs, but these materials usually suffer from defective electrochemical performances and still cannot fully satisfy the increasing demands. $Li_3V_2(PO_4)_3$ (LVP), the typical V-based cathode material, is considered as one of the most promising candidates of cathode materials for LIBs with high operation voltage, good capacity and long cycling life.[12–18] However, the poor kinetic properties of LVP caused by its intrinsic low electronic conductivity (2×10^{-8} S cm^{-1}) and ionic conductivity (10^{-9}–10^{-10} cm^2 s^{-1}) hinder its commercial usage.[19–21] Several approaches have been developed to relieve this issue, such as conductive coating to improve the electronic conductivity of cathodes[22–26] or preparing different nanostructures to reduce Li-ion diffusion pathways.[27–33] These approaches showed limited success, but it still remains a great challenge to seek simple and effective strategies for the fabrication of LVP-based nanostructural cathodes with high-rate capability and long-life performance.

According to the diffusion formula $t = L^2/D$ (where t is the ion diffusion time, L is the ion diffusion distance, and D is the ion diffusion coefficient), electrode materials with the morphology of nanoparticles or nanofibers are very beneficial to improve the rate performance, owing to their short ion diffusion distance.[34,35] Compared to the relatively isolated nanoparticles, nanofibers and nanowires with high conduc-

[a]*Key Laboratory of Mesoscopic Chemistry of MOE and Collaborative Innovation Center of Chemistry for Life Sciences, School of Chemistry and Chemical Engineering, Nanjing University, Nanjing, 210093, China. E-mail: zhongjin@nju.edu.cn*
[b]*Key Laboratory of MEMS of the Ministry of Education, Department of Physics, Southeast University, Nanjing 210096, China. E-mail: xuqingyu@seu.edu.cn*
[c]*College of Chemistry, Chemical Engineering and Materials Science, Zaozhuang University, Zaozhuang, 277160, China*
[d]*College of Engineering and Applied Sciences, Nanjing University, Nanjing, 210093, China*
[e]*Department of Chemistry, Duke University, Durham, North Carolina 27708, USA. E-mail: j.liu@duke.edu*
†Electronic supplementary information (ESI) available. See DOI: 10.1039/c5nr08832a
‡Both authors contributed equally to this work.

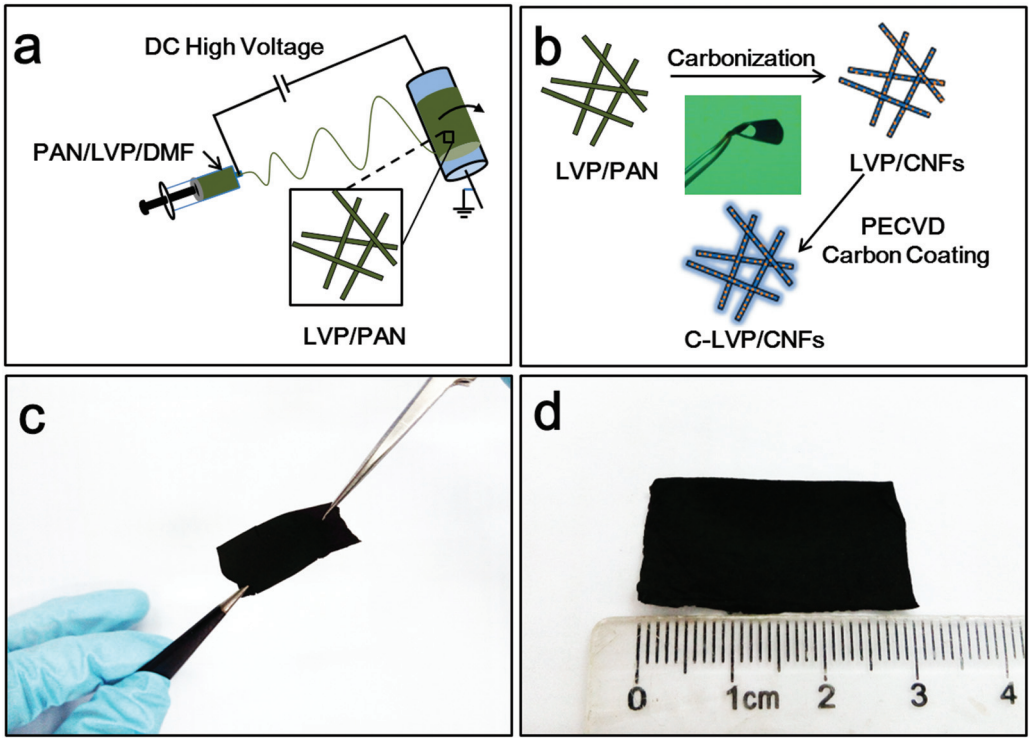

Fig. 1 Schematic diagrams of (a) the electrospinning fabrication of LVP/PAN composite nanofibers and (b) the formation of LVP/CNFs by thermal carbonization and subsequent PECVD carbon-coating. The optical images of as-prepared (c) LVP/CNFs and (d) C-LVP/CNFs were obtained by using a digital camera.

tivity and a continuous electron transport pathway can result in even better electrochemical performances. Electrospinning is a facile and scalable technique to fabricate ultra-fine hierarchical one-dimensional (1D) carbon nanofibers with controllable diameters, aspect ratios, compositions, directions, constructions and so on.[36–39] The as-prepared materials usually exhibit 1D and/or porous hierarchical nanostructures, and have some unique advantages, such as (1) a short Li-ion diffusion distance,[40,41] (2) a continuous electron transport pathway,[42] (3) facile strain relaxation,[10,43] and (4) a significantly increased contact area between the electrode and electrolyte.[44] Therefore, it is very promising to rationally design superior electrode materials by fabricating flexible composite nanofibers implanted with highly-dispersed electroactive nanofillers. These fibrous composite electrodes with different components may be utilized for many practical applications, especially high-rate, high-capacity cathodes and anodes in flexible LIBs for wearable consumer electronics.

Here we present a feasible method based on electrospinning and subsequent annealing to prepare LVP nanoparticle-encapsulated carbon nanofibers (LVP/CNFs) with high flexibility and evenly-distributed monoclinic LVP nanocrystals with a uniform diameter (Fig. 1). Polyacrylonitrile (PAN) was chosen as the carbon precursor for the preparation of LVP/CNFs owing to its good solubility in many organic solvents and high mechanical properties after carbonization. Electrospun PAN nanofibers can be thermally carbonized at high temperatures and under an inert atmosphere to form free-standing nanofabric membranes consisting of carbon nanofibers with high flexibility and a large surface area.[45–47] The integrity and mechanical robustness of carbon nanofabric membranes can still be well maintained with a high loading mass of encapsulated LVP nanoparticles. Furthermore, plasma enhanced chemical vapor deposition (PECVD) of acetylene (C_2H_2) was used to add a smooth thin layer of carbon to further improve the conductivity of carbon-coated LVP/CNFs (C-LVP/CNFs). The high-porosity C-LVP/CNFs with an unobstructed electron/ion pathway are kinetically superior to the rapid transport and insertion/extraction of Li^+, resulting in high ionic conductivity. Moreover, the highly conductive layer of the carbon outer-shell coated by PECVD can further protect the electrochemically-active LVP nanoparticles and prevent the structural degradation of nanofabric electrodes during the lithiation/delithiation processes, thus remarkably improving the cyclic stability and rate performance of the nanofabric electrodes. As a result of the synergistic contributions of all components in this fibrous cathode, the novel C-LVP/CNFs showed excellent electrochemical performances as a flexible cathode material for fast-charging and long-life LIBs.

2. Experimental

2.1. Synthesis of LVP nanoparticles

LVP nanoparticles were prepared by a modified sol–gel method. Typically, 15 mmol $LiOH{\cdot}H_2O$ (AR, ≥99.0%), 10 mmol

NH_4VO_3 (AR, ≥99.0%), and 15 mmol $NH_4H_2PO_4$ (AR, ≥99.0%) were separately dissolved in 50 mL distilled water to prepare NH_4VO_3, LiOH and $NH_4H_2PO_4$ solutions. The above solutions were sequentially added to 50 mL of 0.20 M citric acid solution dropwise and then stirred vigorously at room temperature for 12 h. The mixture was heated in a thermostatic water bath at 80 °C with constant stirring for 6 h to evaporate the excess water until a blue gel was formed. The gel was dried in a vacuum oven at 80 °C for 12 h, and then annealed at 300 °C for 6 h under an Ar atmosphere to obtain powdery LVP nanoparticles.

2.2. Preparation of LVP/CNFs

The as-prepared LVP nanoparticles (0.66 g) were added into an equal weight of 12 wt% PAN/dimethyl formamide (DMF) solution and then ultrasonicated (100 W, Hechuang KH-2200 ultrasonicator, Kunshan) at room temperature for 12 h. The mixture was electrospun under a DC voltage of 18 kV applied between an injector needle (with an inner diameter of 0.7 mm and a flow rate of 2.0 mL h^{-1} precisely controlled by a Longer LSP02-1B syringe pump, Baoding) and a rotating cylindrical aluminum foil collector with a working distance of 12 cm and a rotation speed of 800 rpm, as shown in Fig. 1a. The intermediate composite nanofibers were peeled off from the collector and sintered at 800 °C for 4 h in Ar after heating from room temperature with a heating rate of 2 °C min^{-1} to yield the LVP/CNFs.

2.3. Preparation of C-LVP/CNFs

The LVP/CNFs were coated with a carbon outer-layer by PECVD using C_2H_2 as a carbon precursor (Fig. 1b). The LVP/CNFs were loaded in a ceramic boat and placed into a 1-inch quartz tube furnace (Boyuntong TL1200, Nanjing) with a 13.56 MHz plasma source at a working power of 500 W and a bias of 214–218 V. During the coating process, 100 sccm of C_2H_2 and 300 sccm of H_2 were introduced into the quartz tube at 500 °C under atmospheric pressure for 30 min to obtain C-LVP/CNFs. After the reaction, the gas flow was changed to 300 sccm of Ar and the furnace was cooled to room temperature.

2.4. Structural characterization

Powder X-ray diffraction (XRD) was performed on an X-ray diffractometer (Shimadzu XRD-6000, Cu Kα X-ray source) with step scanning of 0.02° over a 2θ range of 10–60°. The morphological features of LVP/CNFs and C-LVP/CNFs were characterized with a scanning electron microscope (SEM, JEOL JSM-7600F). The components and chemical states of samples were studied by X-ray photoelectron spectroscopy (XPS, Thermo Scientific K-Alpha, Al Kα X-ray source). Thermo-gravimetric analysis (TGA) was carried out on a Mettler-Toledo SDTA851e analyzer. The samples were firstly heated to 110 °C for 1 h to remove any remaining water or solvents and then cooled to room temperature. Subsequently, the samples were heated to 850 °C at 10 °C min^{-1} under a dry air flow of 40 sccm to measure the weight loss.

2.5. Electrochemical measurements

The free-standing LVP/CNF and C-LVP/CNF thin films were directly used as working electrodes without adding any binder, current collector or ancillary materials (Fig. 1c and d). The assembly of coin cells was performed in an Ar-filled glove box by using CR2032 coin-type cells. Pure lithium foils were used as counter electrodes, Celgard-2400 polypropylene membranes were used as separators, and 1 mol L^{-1} $LiPF_6$ in a solution of ethylene carbonate and dimethyl carbonate (EC and DMC, 1 : 1 by volume) served as an electrolyte. Galvanostatic charging/discharging tests were conducted in a voltage cut-off of 3.0–4.3 V (*vs.* Li/Li^+) at different C-rates on a multichannel battery testing system (LAND CT2001A, Wuhan) at room temperature. Electrochemical impedance spectroscopy (EIS) measurements were performed on an electrochemical workstation (Chenhua CHI-760A, Shanghai) with an AC voltage amplitude of 5 mV on the cells in the frequency range from 100 KHz to 10 MHz. The loading mass of LVP active materials was *ca.* 0.8–1.0 mg, and the specific capacity of the electrode was calculated based on the weight of LVP active materials.

3. Results and discussion

The morphologic features of the as-obtained LVP/CNFs and C-LVP/CNFs are shown in Fig. 2. The LVP/CNFs consist of long and continuous composite nanofibers with an evenly-distributed diameter of 220 ± 10 nm (Fig. 2a and b). It was observed that the LVP nanoparticles with an average size of ~50 nm were embedded in the nanofibers uniformly. During the PECVD carbon coating procedure, the precursor C_2H_2 is decomposed and formed as carbon on the surface with the assistance of plasma. According to the mean diameter change of carbon nanofibers before and after PECVD, the thickness of the carbon layer was estimated to be roughly 6–7 nm. The surface of C-LVP/CNFs (Fig. 2d) is much smoother than the original LVP/CNFs (Fig. 2c), owing to the formation of carbon outer-shells. The fibrous morphology of the composite was well-retained after carbon coating, as evidenced from the SEM images (Fig. 2d). Only a few LVP nano-granules were still exposed to the surface of C-LVP/CNFs. TEM and HRTEM were used to investigate the detailed nanostructure of the C-LVP/CNFs. The nanoparticles with the size range of 30–80 nm were embedded and distributed uniformly in the CNFs (Fig. 2e). Further HRTEM observation (Fig. 2f) revealed a lattice distance of 0.363 nm, which was attributed to the (211) planes of LVP.

The crystalline features of LVP/CNFs and C-LVP/CNFs were analyzed by XRD and are presented in Fig. 3a. All the diffraction peaks of both the composites can be assigned to the carbon nanofibers with mainly an amorphous structure and the well-defined monoclinic phase $Li_3V_2(PO_4)_3$ (JCPDS No. 01-072-7074) with high crystallinity. The relative intensity of the characteristic peaks of LVP nanoparticles embedded in C-LVP/CNFs is slightly lower in comparison with those of LVP/CNFs, which may have resulted from the carbon outer-shells covered on the LVP nanoparticles. There is no obvious

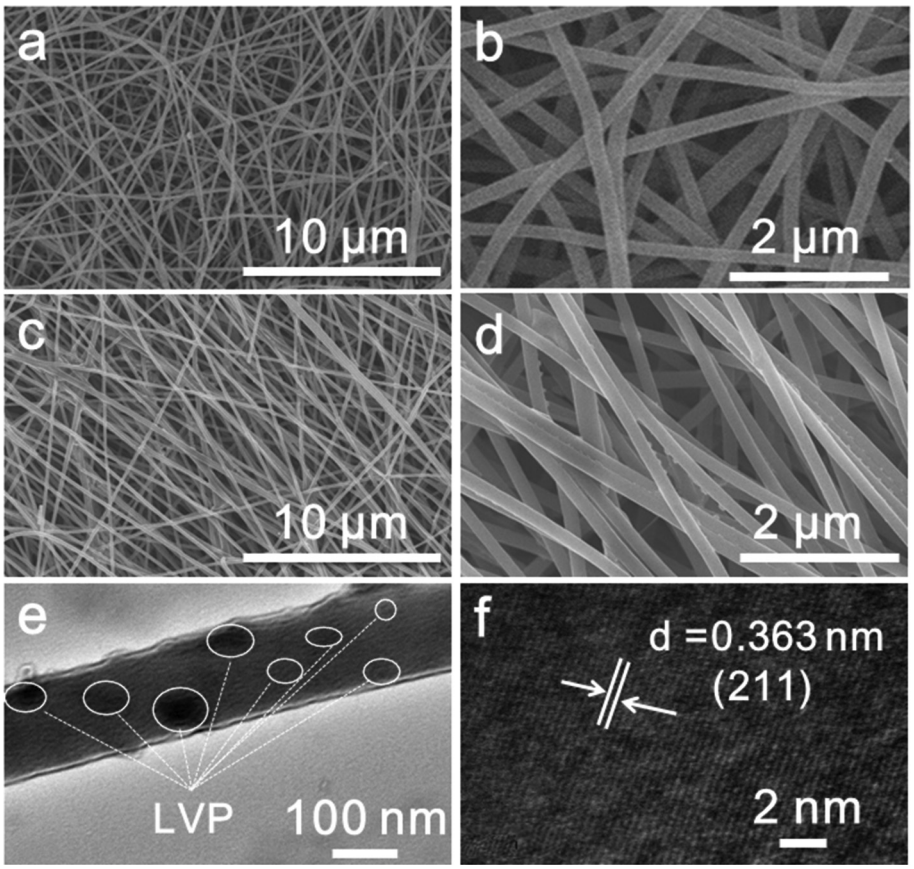

Fig. 2 SEM images of (a, b) LVP-CNFs, (c, d) C-LVP/CNFs. (e) TEM and (f) HRTEM image of C-LVP/CNFs. The particles are entirely embedded into the CNFs. The observed lattice distance of 0.363 nm is attributed to the (211) planes of LVP.

characteristic peak from impurities, suggesting that the compositions of the nanofibers were only LVP and CNFs. TGA was utilized to evaluate the carbon content in the products (Fig. 3b). The weight loss above 350 °C can be mainly ascribed to the oxidation of carbon outer-shells and nanofibers in air. The weight percentage of LVP in the fibrous cathodes can be estimated to be as high as ~85% and ~80% for LVP/CNFs and C-LVP/CNFs, respectively. Further Raman characterization (Fig. S1†) of C-LVP/CNFs and LVP/CNFs revealed the amorphous nature of CNFs and carbon layers coated by PECVD, which is consistent with the results in the literature.[48] XPS was performed to characterize the surface composition of the LVP/CNFs and C-LVP/CNFs. The XPS survey (Fig. 3c) revealed the presence of C, N, O, P and V species. In the high-resolution XPS spectrum of N 1s for LVP/CNFs and C-LVP/CNFs (Fig. 3d), a "pyridinic" –N═ peak at ~398.6 eV and a "graphitic" –N< peak at ~400.7 eV were observed.[45] The atomic ratio of N : C on the surface of LVP/CNFs was measured as ~0.11; the high nitrogen content in the LVP/CNFs was mainly derived from the nitrile (–C≡N) groups in the PAN precursor. After the PECVD treatment, the atomic ratio of N : C decreased to ~0.026 for C-LVP/CNFs, owing to the uniform coverage of carbon outer-shells. The binding energy of O 1s in LVP/CNFs and C-LVP/CNFs is around 531.5 eV, as shown in Fig. 3e, which is due to the oxygen predominantly bonded with V or P atoms. A shoulder peak at 531.0 eV for LVP/CNFs may be attributed to the C═O groups. While an additional O 1s peak of C-LVP/CNFs at 533.1 eV should be caused by the surface O–H groups or adsorbed water, similar to the values reported for O 1s in $LiFePO_4$ (533.2 eV).[49] The binding energy of the V $2p_{3/2}$ peak located at ~517.3 eV for C-LVP/CNFs and LVP/CNFs (Fig. 3f) can be ascribed to the oxidation state of V(III) species in LVP nanoparticles.[50,51] This result is also well consistent with those for $LiVPO_4F$ (517.1 ± 0.2 eV)[49] and rGO/$[K_2(VO)_2(HPO_4)_2(C_2O_4)]$ (517.3 ± 0.2 eV).[52]

Fig. 4a depicts the first charge/discharge profiles of C-LVP/CNFs at different current rates (1 C = 133 mA h g^{-1}) in the voltage range of 3.0–4.3 V at room temperature. When the rate was set to 0.5 C, the C-LVP/CNFs exhibited three pairs of charge/discharge plateaus located at around 3.60/3.57, 3.68/3.65, and 4.10/4.06 V, owing to a series of reversible phase transitions during electrochemical reactions. However, the plateaus observed from LVP/CNFs (Fig. 4b) are much more sloping, indicating a lower reversibility of insertion/extraction of lithium ions. The specific capacity of coin-type cells with LVP/CNFs or C-LVP/CNFs as a cathode and lithium foil as an anode was calculated based on the total weight of the active material LVP loaded on the free-standing nanofabric cathodes.

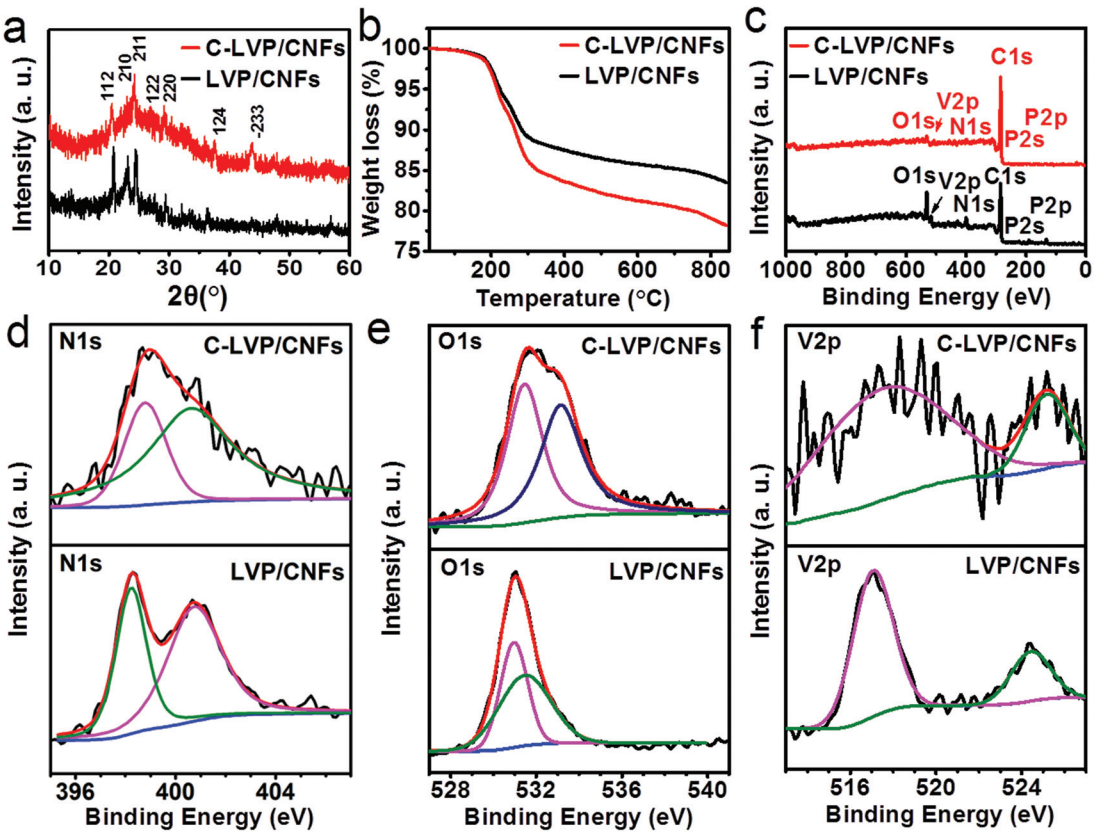

Fig. 3 (a) XRD spectra, (b) TGA profiles and (c) survey XPS curves of LVP/CNFs and C-LVP/CNFs, respectively. High-resolution XPS analysis of (d) N 1s, (e) O 1s, (f) V 2p of LVP/CNFs and C-LVP/CNFs.

The initial discharge capacity of C-LVP/CNFs at the rate of 0.5 C is 128 mA h g^{-1} (close to the theoretical capacity of 133 mA h g^{-1} for LVP), which is much higher than that of LVP/CNFs (107 mA h g^{-1}). The C-LVP/CNF cathodes exhibited a minimal capacity decrease at higher rates, demonstrating their excellent high-rate capability. Even at 10 C, a discharge capacity of 120 mA h g^{-1} (90.5% of the theoretical capacity) was delivered by the C-LVP/CNFs, almost two times higher than that of the LVP/CNFs (64 mA h g^{-1}). When the current rate was increased stepwise from 0.5 C to 10 C, the C-LVP/CNFs still preserved their stable capacities during the entire process (Fig. 4c). About 97.6% of the initial capacity (125 mA h g^{-1}) for C-LVP/CNFs was recovered after the current rate turned back to 0.5 C, indicating a very good electrochemical reversibility. In contrast, the LVP/CNFs present a much lower high-rate performance that can only reach 62 mA h g^{-1} at 10 C. To further investigate the effect of carbon coating on the electrochemical performance of LVP/CNFs, EIS measurements were performed on C-LVP/CNFs and LVP/CNFs before cycling (Fig. 4d). The high-to-middle frequency semicircles in the Nyquist impedance plots correspond to the impedance of Li^+ diffusion in the surface layer (R_s), while the middle-to-low frequency regions refer to the charge transfer (R_{ct}) and the interfacial capacitance across the electrode/electrolyte interface as a constant-phase element (CPE). The inclined lines in the low-frequency region represent the Warburg impedance (Z_w) related to the diffusive resistance of the electrolyte in the interior part of the electrode surface.[50] The charge transfer resistance (R_{ct}) of C-LVP/CNFs is 61 Ω, much smaller than that of LVP/CNFs (152 Ω). Moreover, the impedance characteristics of C-LVP/CNFs and LVP/CNFs at various charge states were also investigated. As shown in Fig. S2,† in the first charge process, with the increase of charge voltage (from 3.0 to 4.3 V *vs.* Li/Li^+), the charge-transfer resistances (R_{ct}) of both C-LVP/CNF and LVP/CNF electrodes increased (from 65 to 316 Ω for C-LVP/CNFs, and from 158 to 489 Ω for LVP/CNFs), which may be attributed to the formation of the SEI film as well as the electronic resistance increase of the active material and the ionic resistance increase of the electrolyte filled in the composite electrode.[53,54] In contrast, in the 10th charge process, the R_{ct} value decreased (from 148 to 59 Ω for C-LVP/CNFs, and from 268 to 153 Ω for LVP/CNFs) along with the increase of charge voltage. This phenomenon may be associated with the electrochemical activation of CNFs and carbon layers. It should be noted that the C-LVP/CNF electrode exhibits a much smaller R_{ct} than the LVP/CNF electrode under the same conditions, which may be attributed to the existence of carbon shells on LVP/CNFs. These indicate that the electronic conductivity of C-LVP/CNFs was further improved by carbon coating, which was also well reflected in the electrochemical cycling

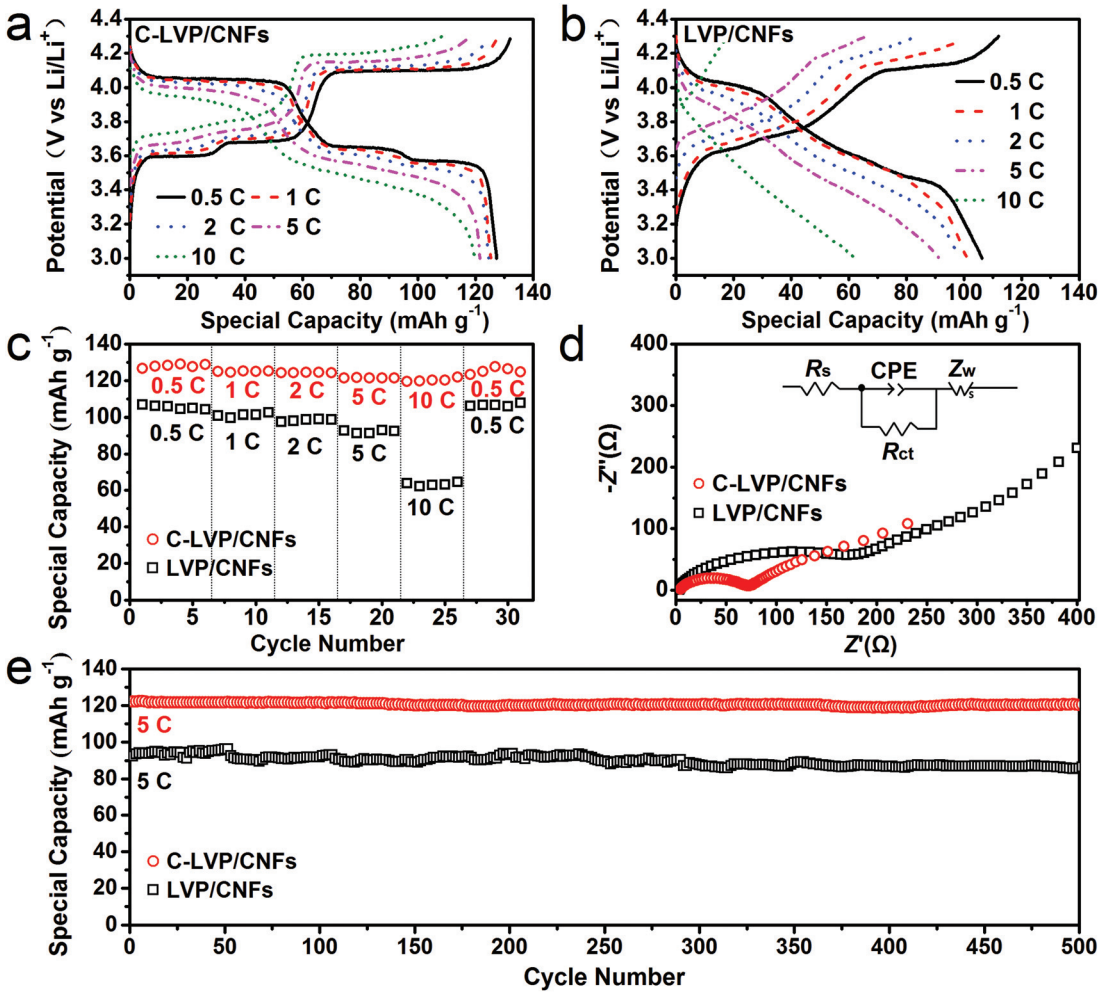

Fig. 4 Charge/discharge profiles of (a) C-LVP/CNFs, (b) LVP/CNFs at different current rates (1 C = 133 mA h g^{-1}). (c) Rate performance of C-LVP/CNFs and LVP/CNFs. (d) Nyquist plots of LVP/CNFs and C-LVP/CNFs. The inset shows the equivalent circuits. (e) Long-term cycling performance of LVP/CNFs and C-LVP/CNFs at 5 C.

performance. The long-term cycling performance of both C-LVP/CNFs and LVP/CNFs at a high rate of 5 C is shown in Fig. 4e. The cathodes of C-LVP/CNFs delivered an initial discharge capacity of 122 mA h g^{-1} and still maintained a remarkable capacity of 121 mA h g^{-1} after 500 cycles, corresponding to a capacity retention as high as 98.9%. On comparison, the LVP/CNFs cycled at the same rate retained a discharge capacity of 85 mA h g^{-1} (92.8% of the initial capacity) after 500 cycles. In addition, to investigate the influence of the loading mass on the electrochemical performances of the C-LVP/CNF electrode, the loading mass of the LVP active material in C-LVP/CNFs was further increased to *ca.* 5.5 mg. Remarkably, electrochemical measurements (Fig. S3†) revealed similar results (118 mA h g^{-1} after 100 cycles at 5 C), suggesting that the C-LVP/CNF material can still maintain a high electrochemical performance when the loading mass is relatively high.

On the basis of the above results, it can be deduced that the carbon coating by PECVD greatly improved the rate capability and cycling performance of the nanofabric cathodes. Firstly, the electronic conductivity has been further increased by the presence of the carbon outer layer, which is clearly seen from the electrochemical properties of C-LVP/CNFs at high current densities. Improvement in conductivity enabled more facile Li^+ intercalation/de-intercalation during the charge/discharge processes, thus remarkably enhancing the rate performance. Secondly, the homogeneous coating of the carbon shell can effectively protect the electrochemically-active LVP nanoparticles from side reactions with electrolytes.[37] Therefore, the possible structural degradation of the electrode material during the lithiation/delithiation processes was prevented and the cyclic stability was significantly elevated.

4. Conclusion

In summary, we have developed a feasible and effective strategy based on electrospinning, thermal annealing and PECVD to fabricate flexible composite nanofabric electrodes with

uniformly embedded LVP nanoparticles for LIBs. In comparison with bare LVP/CNFs, the cathodes of C-LVP/CNFs obtained by further applying the PECVD carbon-coating process demonstrated much better cycling stability, capacity retention and excellent rate capability. It proves that a conductive carbon outer-layer of composite cathodes can greatly enhance the rate capability and long-term cyclability. Moreover, we expect that the method reported in this work could be extended to the preparation of other novel free-standing composite electrode materials with high integrity for application in high-performance LIBs and other wearable energy storage devices.

Acknowledgements

This work is supported by the National Thousand Young Talents Program of China, the Young Scientists Project of National Basic Research Program of China (973 Program No. 2015CB659300), the National Natural Science Foundation of China (NSFC Grant No. 21403105; No. 21573108; No. 51172044; No. 51471085), the China Postdoctoral Science Foundation (Grant No. 2015M581769), the Natural Science Foundation for Young Scholars of Jiangsu Province (Project No. BK20150571; No. BK20150583; No. BK20151400), the Fundamental Research Funds for the Central Universities and a project funded by the Priority Academic Program Development of Jiangsu Higher Education Institutions (PAPD).

References

1 J.-M. Tarascon and M. Armand, *Nature*, 2001, **414**, 359–367.
2 M. J. Armstrong, C. O'Dwyer, W. J. Macklin and J. D. Holmes, *Nano Res.*, 2014, **7**, 1–62.
3 Y. Gogotsi and P. Simon, *Science*, 2011, **334**, 917–918.
4 B. Dunn, H. Kamath and J. M. Tarascon, *Science*, 2011, **334**, 928–935.
5 J. B. Goodenough and K. S. Park, *J. Am. Chem. Soc.*, 2013, **135**, 1167–1176.
6 C. K. Chan, H. Peng, G. Liu, K. Mcilwrath, X. F. Zhang, R. A. Huggins and Y. Cui, *Nat. Nanotechnol.*, 2008, **3**, 31–35.
7 M. Nagarathinam, K. Saravanan, E. J. H. Phua, M. V. Reddy, B. V. R. Chowdari and J. J. Vittal, *Angew. Chem., Int. Ed.*, 2012, **51**, 5866–5870.
8 A. S. Hameed, M. Nagarathinam, M. Schreyer, M. V. Reddy, B. V. R. Chowdari and J. J. Vittal, *J. Mater. Chem. A*, 2013, **1**, 5721–5726.
9 A. S. Hameed, M. V. Reddy, N. Sarkar, B. V. R. Chowdari and J. J. Vittal, *RSC Adv.*, 2015, **5**, 60630–60637.
10 Y. Wu, P. Zhu, X. Zhao, M. V. Reddy, S. Peng, B. V. R. Chowdaric and S. Ramakrishna, *J. Mater. Chem. A*, 2013, **1**, 852–859.
11 A. S. Hameed, M. Nagarathinam, M. V. Reddy, B. V. R. Chowdari and J. J. Vittal, *J. Mater. Chem.*, 2012, **22**, 7206–7213.
12 B. H. Huang, S.-C. Yin, T. Kerr, N. Taylor and L. F. Nazar, *Adv. Mater.*, 2002, **14**, 1525–1528.
13 J. Kim, J. K. Yoo, Y. S. Jung and K. Kang, *Adv. Energy Mater.*, 2013, **3**, 1004–1007.
14 S.-C. Yin, H. Grondey, P. Strobel, M. Anne and L. F. Nazar, *J. Am. Chem. Soc.*, 2003, **125**, 10402–10411.
15 Y. Zhou, X. Rui, W. Sun, Z. Xu, Y. Zhou, W. J. Ng, Q. Yan and E. Fong, *ACS Nano*, 2015, **9**, 4628–4635.
16 R. V. Hagen, A. Lepcha, X. Song, W. Tyrra and S. Mathur, *Nano Energy*, 2013, **2**, 304–313.
17 D. Morgan, G. Ceder, M. Y. Saïdi, J. Barker, J. Swoyer, H. Huang and G. Adamson, *Chem. Mater.*, 2002, **14**, 4684–4693.
18 S.-C. Yin, H. Grondey, P. Strobel, H. Huang and L. F. Nazar, *J. Am. Chem. Soc.*, 2003, **125**, 326–327.
19 Y. Luo, X. Xu, Y. Zhang, Y. Pi, Y. Zhao, X. Tian, Q. An, Q. Wei and L. Mai, *Adv. Energy Mater.*, 2014, **1400107**, 1–8.
20 X. Zhang, N. Bçckenfeld, F. Berkemeier and A. Balducci, *ChemSusChem*, 2014, **7**, 1710–1718.
21 D. Han, S. Lim, Y. Kim, S. H. Kang, Y. C. Lee and Y. Kang, *Chem. Mater.*, 2014, **6**, 3644–3650.
22 J. Wang and X. Sun, *Energy Environ. Sci.*, 2012, **5**, 5163–5185.
23 H. Ji, L. Zhang, M. T. Pettes, H. Li, S. Chen, L. Shi, R. Piner and R. S. Ruoff, *Nano Lett.*, 2012, **12**, 2446–2451.
24 Q. Liu, Z. Li, Y. Liu, H. Zhang, Y. Ren, C. Sun, W. Lu, Y. Zhou, L. Stanciu, E. A. Stach and J. Xie, *Nat. Commun.*, 2015, **6127**, 1–10.
25 B. L. Hu, F. Wu, C. Lin, A. N. Khlobystov and L. Li, *Nat. Commun.*, 2013, **1687**, 1–7.
26 B. S. W. Oh, S. Myung, S. Oh, K. H. Oh, K. Amine, B. Scrosati and Y. Sun, *Adv. Mater.*, 2010, **22**, 4842–4845.
27 Q. Wei, Q. An, D. Chen, L. Mai, S. Chen, Y. Zhao, K. M. Hercule, L. Xu, A. Minhas-Khan and Q. Zhang, *Nano Lett.*, 2014, **14**, 1042–1048.
28 X. Zhang, F. Cheng, J. Yang and J. Chen, *Nano Lett.*, 2013, **13**, 2822–2825.
29 L. Q. Mai, Q. L. Wei, Q. Y. An, X. C. Tian, Y. L. Zhao, X. Xu, L. Xu, L. Chang and Q. J. Zhang, *Adv. Mater.*, 2013, **25**, 2969–2973.
30 H. Liu and W. Yang, *Energy Environ. Sci.*, 2011, **4**, 4000–4008.
31 H.-W. Lee, P. Muralidharan, R. Ruffo, C. M. Mari, Y. Cui and D. K. Kim, *Nano Lett.*, 2010, **10**, 3852–3856.
32 L. Mai, L. Xu, C. Han, X. Xu, Y. Luo, S. Zhao and Y. Zhao, *Nano Lett.*, 2010, **10**, 4750–4755.
33 E. Hosono, T. Kudo, I. Honma, H. Matsuda and H. Zhou, *Nano Lett.*, 2009, **9**, 1045–1051.
34 B. Kang and G. Ceder, *Nature*, 2009, **458**, 190–193.
35 H. Zhang, X. Yu and P. V. Braun, *Nat. Nanotechnol.*, 2011, **6**, 277–281.
36 Y. Wu, P. Zhu, M. V. Reddy, B. V. R. Chowdari and S. Ramakrishna, *ACS Appl. Mater. Interfaces*, 2014, **6**, 1951–1958.
37 A. Le Viet, M. V. Reddy, R. Jose, B. V. R. Chowdari and S. Ramakrishna, *Electrochim. Acta*, 2011, **56**, 1518–1528.
38 A. L. Viet, M. V. Reddy, R. Jose, B. V. R. Chowdari and S. Ramakrishna, *J. Phys. Chem. C*, 2010, **114**, 664–671.

39 A. L. Viet, R. Jose, M. V. Reddy, B. V. R. Chowdari and S. Ramakrishna, *J. Phys. Chem. C*, 2010, **114**, 21795–21800.
40 M. V. Reddy, R. Jose, A. L. Viet, K. I. Ozoemena, B. V. R. Chowdari and S. Ramakrishna, *Electrochim. Acta*, 2014, **128**, 198–202.
41 P. Zhu, Y. Wu, M. V. Reddy, A. S. Nair, B. V. R. Chowdarid and S. Ramakrishna, *RSC Adv.*, 2012, **2**, 531–537.
42 C. T. Cherian, J. Sundaramurthy, M. V. Reddy, P. S. Kumar, K. Mani, D. Pliszka, C. H. Sow, S. Ramakrishna and B. V. R. Chowdari, *ACS Appl. Mater. Interfaces*, 2013, **5**, 9957–9963.
43 M. V. Reddy, R. Jose, T. H. Teng, B. V. R. Chowdari and S. Ramakrishna, *Electrochim. Acta*, 2010, **55**, 3109–3117.
44 G. Binitha, M. S. Soumya, A. A. Madhavan, P. Praveen, A. Balakrishnan, K. R. V. Subramanian, M. V. Reddy, S. V. Nair, A. S. Nair and N. Sivakumar, *J. Mater. Chem. A*, 2013, **1**, 11698–11704.
45 Y. Qiu, J. Yu, T. Shi, X. Zhou, X. Bai and J. Y. Huang, *J. Power Sources*, 2011, **196**, 9862–9867.
46 D. Zhang, A. B. Karki, D. Rutman, D. P. Young, A. Wang, D. Cocke, T. H. Ho and Z. Guo, *Polymer*, 2009, **50**, 4189–4198.
47 L. Zeng, W. Zeng, Y. Jiang, X. Wei, W. Li, C. Yang, Y. Zhu and Y. Yu, *Adv. Energy Mater.*, 2014, **1401377**, 1–10.
48 Y. L. Cheah, R. V. Hagen, V. Aravindan, R. Fiz, S. Mathur and S. Madhavi, *Nano Energy*, 2013, **2**, 57–64.
49 M. V. Reddy, G. V. S. Rao and B. V. R. Chowdari, *J. Power Sources*, 2010, **195**, 5768–5774.
50 R. Zhang, Y. Zhang, K. Zhu, F. Du, Q. Fu, X. Yang, Y. Wang, X. Bie, G. Chen and Y. Wei, *ACS Appl. Mater. Interfaces*, 2014, **6**, 12523–12530.
51 N. Membreño, K. Park, J. B. Goodenough and K. J. Stevenson, *Chem. Mater.*, 2015, **27**, 3332–3340.
52 A. S. Hameed, M. V. Reddy, M. Nagarathinam, T. Runčevski, R. E. Dinnebier, S. Adams, B. V. R. Chowdari and J. J. Vittal, *Sci. Rep.*, 2015, **5**, 16270.
53 M. V. Reddy, G. V. S. Rao and B. V. R. Chowdari, *J. Mater. Chem.*, 2011, **21**, 10003–10011.
54 M. V. Reddy, B. L. W. Wen, K. P. Loh and B. V. R. Chowdari, *ACS Appl. Mater. Interfaces*, 2013, **5**, 7777–7785.